AIAA SciTech Forum
4-8 January 2016, San Diego, California, USA
57th AIAA/ASCE/AHS/ASC Structures, Structural Dynamics, and Materials Conference

10.2514/6.2016-0418

Rapid Multi-Objective Aerodynamic Design Using Co-Kriging and Space Mapping

Slawomir Koziel[1], and Yonatan A. Tesfahunegn[2]
Engineering Optimization & Modeling Center, Reykjavik University, Menntavegur 1, 101 Reykjavik, Iceland

Anand Amrit[3], and Leifur Leifsson[4]
Iowa State University, Ames, Iowa 50011

In this paper, a procedure for computationally feasible multi-objective design optimization of aerodynamic surfaces is presented. Our approach exploits multi-fidelity aerodynamics models as well as a multi-objective evolutionary algorithm (MOEA). For the sake of cost reduction, the initial Pareto front is obtained by optimizing a fast kriging surrogate model using MOEA. The surrogate is constructed from sampled low-fidelity model which is pre-conditioned using high-fidelity model data and space mapping. The surrogate is then iteratively refined by enhancing it using high-fidelity model data points sampled along the Pareto set using co-kriging. The process is continued until the Pareto front representation produced by the surrogate aligns with the high-fidelity verification samples. The proposed method allows us to obtain—at a low computational cost—a set of aerodynamic geometries representing trade-offs between the figures of merit. Our approach is illustrated on the design of airfoil shapes in transonic flow at constant lift and obtaining the Pareto front for the drag and pitching moment coefficients.

I.   Introduction

Shape optimization is an important part of the design of aerodynamic components such as aircraft wings and turbine blades.[1,2] Nowadays, the use of high-fidelity computational fluid dynamic (CFD) simulations is widespread in aerodynamic design. While searching for an improved design using CFD-based parameter sweeps and engineering experience is still a common practice, design automation using numerical optimization techniques is becoming more and more popular[3-6]. Various methods and algorithms are available, from conventional, gradient-based algorithms[7], including those utilizing cheap adjoint sensitivities[8,9], to more and more popular surrogate-based optimization techniques[10-15] that offer efficient global optimization and substantial reduction of the design cost as compared to traditional methods[12].

Aerodynamic shape optimization is inherently a multi-objective problem. In many cases, a primary objective (e.g., drag coefficient minimization) may be selected through a priori preference articulation, whereas the others (e.g., lift coefficient) can be handled through design constraints. This allows for solving the problem as a single-objective one. Sometimes, however, this is neither possible nor convenient, e.g., when gaining knowledge about possible trade-offs between competing objectives is important. In those situations genuine multi-objective optimization is necessary. Typically, a solution to multi-objective design is represented as a so-called Pareto front, which represents the set of the best possible designs which are non-commensurable in the conventional (single-objective sense)[16]. The most popular multi-objective optimization methods include multi-objective evolutionary algorithms (MOEAs)[17-19] because these methods are capable of yielding the entire representation of the Pareto front in a single algorithm run. Unfortunately, computational complexity of MOEAs is high due to the fact that a (usually large) set of designs is being processed in each iteration of the algorithm. This may be prohibitive, particularly if high-fidelity CFD simulations are used to evaluate the airfoil/wing under design.

---

[1] Professor, School of Science and Engineering, Senior Member AIAA.
[2] Post-doctoral Fellow, School of Science and Engineering, Member AIAA.
[3] Graduate Student, Department of Aerospace Engineering, Student Member AIAA.
[4] Assistant Professor, Department of Aerospace Engineering, Senior Member AIAA.

Recently[20] a multi-objective procedure exploiting low-fidelity CFD simulations, space mapping, and MOEAs has been proposed, where, in order to reduce the computational cost of the design process, a fast kriging surrogate model (constructed by approximating the low-fidelity CFD simulation data of the airfoil) was exploited. The surrogate was corrected using sparsely sampled high-fidelity CFD data and parameterized output space mapping[21] and, subsequently, optimized using MOEA. Space mapping correction has been further utilized to enhance the surrogate model along the Pareto front by incorporating more high-fidelity data samples. A potential drawback of the method[20] is that approximation capability of the space mapping (SM) correction is of limited flexibility due to a fixed number of SM parameters.

In this paper, we propose an alternative approach, where, the initial Pareto set is also obtained by optimizing the kriging surrogate model constructed from the low-fidelity CFD data samples (potentially enhanced by space mapping corrections), however, the surrogate refinement is realized with the high-fidelity CFD data samples blended into the model using co-kriging. This allows us to improve the surrogate model flexibility and convergence properties of the optimization algorithm. Our approach is illustrated using an example of a transonic airfoil at fixed lift.

II. Multi-Objective Airfoil Design

In this section, the airfoil characteristics and design variables are described. We formulate the multi-objective airfoil design problem and define the high- and low-fidelity aerodynamics models.

A. Multi-objective Design Formulation

Let $\mathbf{f}(\mathbf{x}) = [C_{l,f}(\mathbf{x})\ C_{d,f}(\mathbf{x})\ C_{m,f}(\mathbf{x})]^T$ be the attributes of the airfoil obtained by an accurate high-fidelity aerodynamics simulation model. Here, $C_{l,f}$, $C_{d,f}$, and $C_{m,f}$ are the lift, drag, and pitching moment coefficients, respectively, and $\mathbf{x}$ is the vector of designable parameters. Let $F_k(\mathbf{x})$, $k = 1, \ldots, N_{obj}$, be a kth design objective of interest. A typical performance objective would be to minimize the drag coefficient, in which case $F_k(\mathbf{x}) = C_{d,f}$. Another objective would be to maximize lift, in which case $F_k(\mathbf{x}) = 1/C_{l,f}$ or $F_k(\mathbf{x}) = -C_{l,f}$. Moreover, another objective could be to either minimize or maximize the pitching moment coefficient, i.e., $F_k(\mathbf{x}) = C_{m,f}$ or $F_k(\mathbf{x}) = -C_{m,f}$, respectively.

If $N_{obj} > 1$ then any two designs $\mathbf{x}^{(1)}$ and $\mathbf{x}^{(2)}$ for which $F_k(\mathbf{x}^{(1)}) < F_k(\mathbf{x}^{(2)})$ and $F_l(\mathbf{x}^{(2)}) < F_l(\mathbf{x}^{(1)})$ for at least one pair $k \neq l$, are not commensurable, i.e., none is better than the other in the multi-objective sense. We define Pareto dominance relation $\prec$ (see, e.g., Fonseca[16]), saying that for the two designs $\mathbf{x}$ and $\mathbf{y}$, we have $\mathbf{x} \prec \mathbf{y}$ ($\mathbf{x}$ dominates $\mathbf{y}$) if $F_k(\mathbf{x}) < F_k(\mathbf{y})$ for all $k = 1, \ldots, N_{obj}$. The goal of the multi-objective optimization if to find a representation of a so-called Pareto front (of Pareto-optimal set) $\mathbf{X}_P$ of the design space $\mathbf{X}$, such that for any $\mathbf{x} \in \mathbf{X}_P$, there is no $\mathbf{y} \in \mathbf{X}$ for which $\mathbf{y} \prec \mathbf{x}$ (Fonseca[16]). In practice, the Pareto front gives us information about possible trade-offs between the competing objectives, e.g., what is the minimum drag for given value of the lift coefficient. Having reasonable representation of the Pareto front is therefore indispensable in making various design decisions.

It should be emphasized that an important part of the multi-objective design is a decision making process, i.e., selection of a specific design from a number of alternatives contained in the Pareto front, based on given preferences concerning, among others, importance of particular objectives. In this work, we only focus on the methodology for obtaining the Pareto front itself. The subsequent decision making process is beyond the scope of this paper.

B. Design Variables

The airfoil shapes are defined by the B-spline parametrization method[22], and the airfoil surfaces are written in parametric form as

$$x(t) = \sum_{i=1}^{n+1} X_i N_{i,k}(t), \ \ z(t) = \sum_{i=1}^{n+1} Z_i N_{i,k}(t), \tag{1}$$

where (x,z) are the Cartesian coordinates of the surface, $N_{i,k}$ is the B-spline basis function of order k, (X_i, Z_i) are the coordinates of the B-spline control polygon, and $n+1$ is the total number of control points. The control points are used as design variables, as shown in Fig. 1, where each designable control point is free to move in the vertical direction only. Thus, the design variable vector is $\mathbf{x} = [Z_1\ Z_2\ \ldots\ Z_{n+1}]^T$ and the corresponding X_i are fixed during the optimization. In this work, we use 8 control points, 4 for each surface (as shown in Fig. 1).
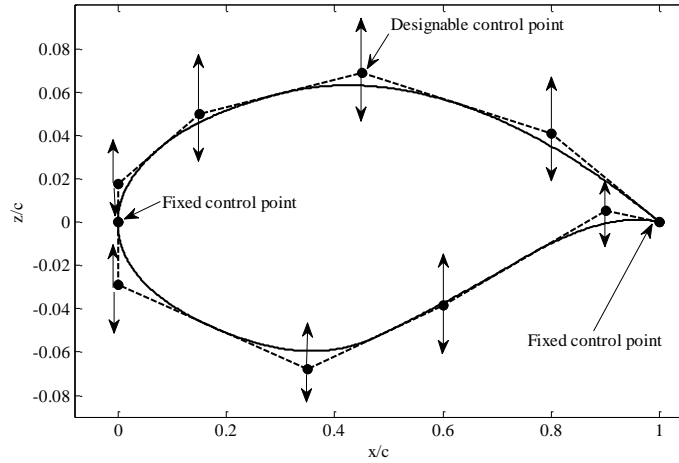
Figure 1.   Airfoil shape parameterization using B-spline curves[22] for the upper and lower surfaces.

C. Aerodynamics Models

The Stanford University Unstructured (SU^2) computer code[23] is utilized for the fluid flow simulations. The steady compressible Euler equations are solved with an implicit density-based formulation. The convective fluxes are calculated using the second order Jameson-Schmidt-Turkel (JST) scheme[24]. Three multi-grid levels are used for solution acceleration. Asymptotic convergence to a steady state solution is obtained in each case. The flow solver convergence criterion is the one that occurs first of the two: (i) the change in the drag coefficient value over the last 100 iterations is less than 10^{-4}, or (ii) a maximum number of iterations of 1,000 is met.

An O-type computational mesh is generated using Pointwise[25] (see Fig. 2). The farfield boundary is set 55 chord lengths away from the airfoil surface. The mesh density is controlled by the number of cells on the airfoil surface and the number of cells normal to the surface. Distance to the first grid point is $0.001c$. The results of a grid convergence study, given in Table 1, revealed that the 512×512 mesh (shown number 5 in the table) is required for convergence within 0.2 drag counts (1 drag count is $\Delta C_d = 10^{-4}$) when compared with the next mesh. The flow simulation for Mesh 5 takes about 54 minutes. This time includes several simulations to obtain the desired lift coefficient by varying the angle of attack. Typically, 3 to 4 simulations are required.

For the multi-objective optimization studies, Mesh 5 will be used as the high-fidelity model **f**, and Mesh 3 as the low-fidelity model **c** (used only for space mapping and manifold mapping). For the low-fidelity model, the maximum number of solver iterations is set to 500. Figure 3(a) shows the solver convergence of the low-fidelity model, and Fig. 3(b) gives a comparison of the low- and the high-fidelity models. The comparison indicates that the low-fidelity model may be a relatively good representation of the high-fidelity one.
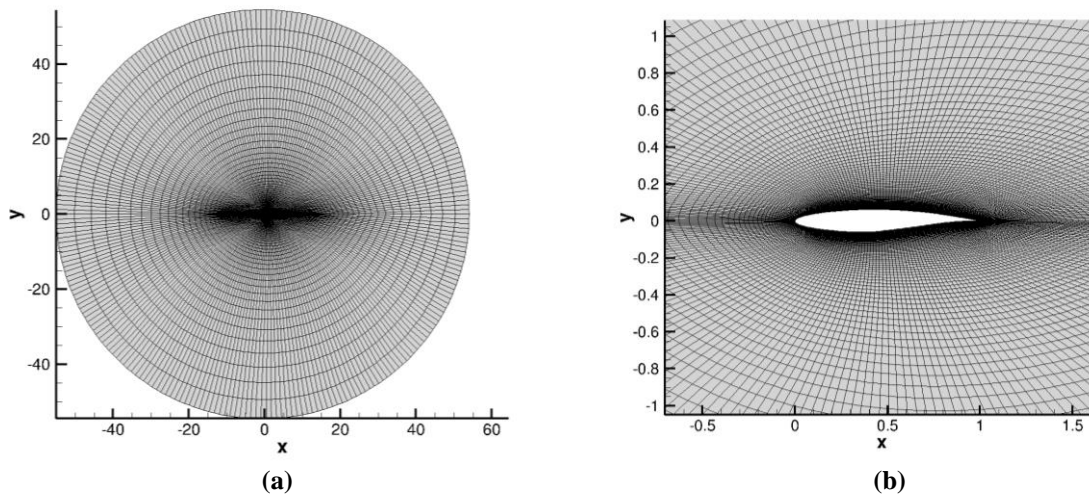

(a)   **(b)**

Figure 2.   Visualization of the computational mesh: (a) farfield view, (b) a view close to the surface.

Table 1.   Grid convergence study of the high-fidelity model for RAE 2822 at $M_\infty = 0.734$ and $C_l = 0.824$.

Mesh	Grid Size	C_l (cts)	C_d (cts)	$C_{m,c/4}$	Simulation Time* (min)
1	32×32 (1,922)	82.40	166.61	-0.0889	0.75
2	64×64 (7,938)	82.40	127.52	-0.0850	1.83
3	128×128 (32,258)	82.40	91.59	-0.1125	8.25
4	256×256 (130,050)	82.40	77.74	-0.1286	25.18
5	512×512 (522,242)	82.40	77.49	-0.1285	54.30
6	$1,024 \times 1,024$ (2,093,058)	82.40	77.30	-0.1287	140.64

(a)	(b)
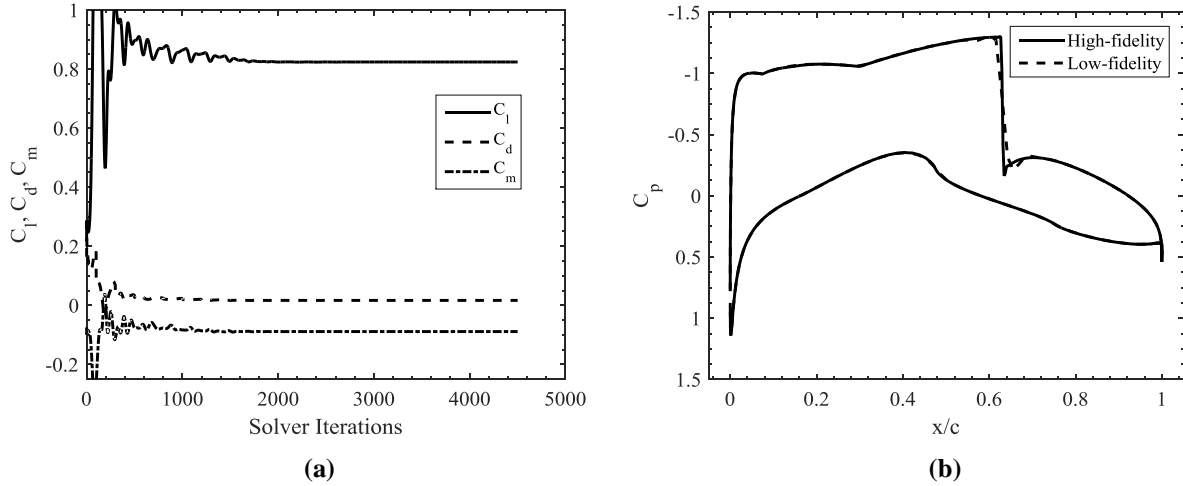
Figure 3.   Simulation results for RAE 2822 at $M = 0.734$ and $C_l = 0.824$: (a) the evolution of the lift, drag, and pitching moment coefficients obtained by the low-fidelity model; (b) a comparison of the pressure distributions obtained by the high- and low-fidelity models.

III.   Surrogate-based Multi-objective Design Optimization

Here, construction of the surrogate model utilized for multi-objective airfoil design is described along with the multi-objective optimization procedure. The numerical results are presented in Section IV.

A. Surrogate Model Construction

The main optimization engine utilized here for Pareto front identification is multi-objective evolutionary algorithm[17] (EA). Due to excessive computational cost of population-based procedures such as EAs, it is not practical to apply evolutionary search directly at the level of expensive CFD simulation model $\mathbf{f}(\mathbf{x}) = [C_{d.f}(\mathbf{x})\ C_{m.f}(\mathbf{x})]^T$ (the lift coefficient $C_{l.f}(\mathbf{x})$ is kept constant by implicitly varying the angle of attack). Instead, we exploit a faster representation of the high-fidelity model, which is a surrogate constructed as follows. Let $\mathbf{c}(\mathbf{x}) = [C_{d.c}(\mathbf{x})\ C_{m.c}(\mathbf{x})]^T$ denote the low-fidelity airfoil model, where $C_{d.c}$ and $C_{m.c}$ are the drag and pitching moment coefficients obtained by the low-fidelity CFD model (the low-fidelity lift coefficient $C_{l.c}(\mathbf{x})$ is kept constant by implicitly varying the angle of attack). The description and setup of the high- and low-fidelity models has been described in Sec. II.C. The surrogate model is constructed in two steps:

Step 1: Space mapping enhancement of the low-fidelity model. In this step, the initial surrogate model $\mathbf{s}_0(\mathbf{x})$ is obtained by applying a parameterized output space mapping[21,26]. The mapping uses the correction terms that are directly applied to the response components $C_{d.c}(\mathbf{x})$ and $C_{m.c}(\mathbf{x})$ of the low-fidelity model (drag coefficient and pitching moment, respectively). The aerodynamic surrogate model is defined as[21]

$$\mathbf{s}_0(\mathbf{x}) = \mathbf{A}(\mathbf{x}) \circ \mathbf{c}(\mathbf{x}) + \mathbf{D} = [a_d(\mathbf{x})C_{d.c}(\mathbf{x}) + d_d(\mathbf{x})\ \ a_m(\mathbf{x})C_{m.c}(\mathbf{x}) + d_m(\mathbf{x})]^T, \tag{2}$$

where $\circ$ denotes component-wise multiplication. Both the multiplicative and additive correction terms are design-variable-dependent and take the form of

$$\mathbf{A(x)} = [a_{d.0} + [a_{d.1}\ a_{d.2}\ ...\ a_{d.n}]\cdot(\mathbf{x}-\mathbf{x}^0)\quad a_{m.0} + [a_{m.1}\ a_{m.2}\ ...\ a_{m.n}]\cdot(\mathbf{x}-\mathbf{x}^0)]^T,\tag{3}$$

$$\mathbf{D(x)} = [d_{d.0} + [d_{d.1}\ d_{d.2}\ ...\ d_{d.n}]\cdot(\mathbf{x}-\mathbf{x}^0)\quad d_{m.0} + [d_{m.1}\ d_{m.2}\ ...\ d_{m.n}]\cdot(\mathbf{x}-\mathbf{x}^0)]^T,\tag{4}$$

where $\mathbf{x}^0$ is the center of the design space. Response correction parameters $\mathbf{A}$ and $\mathbf{D}$ are obtained as

$$[\mathbf{A},\mathbf{D}] = \arg\min_{[\bar{\mathbf{A}},\bar{\mathbf{D}}]}\sum_{k=1}^{N}\|\mathbf{f}(\mathbf{x}^k) - (\bar{\mathbf{A}}(\mathbf{x}^k)\circ\mathbf{c}(\mathbf{x}^k)+\mathbf{D}(\mathbf{x}^k))\|^2,\tag{5}$$

i.e., the response scaling is supposed to (globally) improve the matching for all training points $\mathbf{x}^k$, $k = 1, ..., N$. Similar correction can be applied to the lift coefficient, however, here (in our numerical example), the lift coefficient is not subjected to the optimization process.

In this work, we use a training set consisting of (*i*) factorial design with $2n + 1$ training points (*n* being the number of design variables) allocated at the center of the design space $\mathbf{x}^0 = (\mathbf{l} + \mathbf{u})/2$ (**l** and **u** being the lower and upper bound for the design variables, respectively), and the centers of its faces, i.e., points with all coordinates but one equal to those of $\mathbf{x}^0$, and the remaining one equal to the corresponding component of **l** or **u**; this sampling scheme is also referred to as the star distribution[12], (*ii*) additional 10 points allocated using the Latin Hypercube Sampling[27]. The only formal requirement for the necessary number of samples is that it is larger than the number of model coefficients to be identified.

The correction parameters $\mathbf{A}$ and $\mathbf{D}$ can be calculated analytically as follows[21]

$$\begin{bmatrix} a_{d.0} \\ a_{d.1} \\ \vdots \\ a_{d.n} \\ d_{d.0} \\ \vdots \\ d_{d.n} \end{bmatrix} = (\mathbf{C}_d^T\mathbf{C}_d)^{-1}\mathbf{C}_d^T\mathbf{F}_d \qquad \begin{bmatrix} a_{m.0} \\ a_{m.1} \\ \vdots \\ a_{m.n} \\ d_{m.0} \\ \vdots \\ d_{m.n} \end{bmatrix} = (\mathbf{C}_m^T\mathbf{C}_m)^{-1}\mathbf{C}_m^T\mathbf{F}_m \tag{6}$$

where

$$\mathbf{C}_d = \begin{bmatrix} C_{d.c}(\mathbf{x}^1) & C_{d.c}(\mathbf{x}^1)\cdot(x_1^1-x_1^0) & \cdots & C_{d.c}(\mathbf{x}^1)\cdot(x_n^1-x_n^0) & 1 & (x_1^1-x_1^0) & \cdots & (x_n^1-x_n^0) \\ C_{d.c}(\mathbf{x}^2) & C_{d.c}(\mathbf{x}^2)\cdot(x_1^2-x_1^0) & \cdots & C_{d.c}(\mathbf{x}^2)\cdot(x_n^2-x_n^0) & 1 & (x_1^1-x_1^0) & \cdots & (x_n^1-x_n^0) \\ \vdots & \vdots & \ddots & \vdots & \vdots & \vdots & \vdots & \vdots \\ C_{d.c}(\mathbf{x}^N) & C_{d.c}(\mathbf{x}^N)\cdot(x_1^N-x_1^0) & \cdots & C_{d.c}(\mathbf{x}^N)\cdot(x_n^N-x_n^0) & 1 & (x_1^1-x_1^0) & \cdots & (x_n^1-x_n^0) \end{bmatrix} \tag{7}$$

$$\mathbf{F}_d = \begin{bmatrix} C_{d.f}(\mathbf{x}^1) & C_{d.f}(\mathbf{x}^2) & ... & C_{d.f}(\mathbf{x}^N) \end{bmatrix}^T \tag{8}$$

$$\mathbf{C}_m = \begin{bmatrix} C_{m.c}(\mathbf{x}^1) & C_{m.c}(\mathbf{x}^1)\cdot(x_1^1-x_1^0) & \cdots & C_{m.c}(\mathbf{x}^1)\cdot(x_n^1-x_n^0) & 1 & (x_1^1-x_1^0) & \cdots & (x_n^1-x_n^0) \\ C_{m.c}(\mathbf{x}^2) & C_{m.c}(\mathbf{x}^2)\cdot(x_1^2-x_1^0) & \cdots & C_{m.c}(\mathbf{x}^2)\cdot(x_n^2-x_n^0) & 1 & (x_1^1-x_1^0) & \cdots & (x_n^1-x_n^0) \\ \vdots & \vdots & \ddots & \vdots & \vdots & \vdots & \vdots & \vdots \\ C_{m.c}(\mathbf{x}^N) & C_{m.c}(\mathbf{x}^N)\cdot(x_1^N-x_1^0) & \cdots & C_{m.c}(\mathbf{x}^N)\cdot(x_n^N-x_n^0) & 1 & (x_1^1-x_1^0) & \cdots & (x_n^1-x_n^0) \end{bmatrix} \tag{9}$$

$$\mathbf{F}_m = \begin{bmatrix} C_{m.f}(\mathbf{x}^1) & C_{m.f}(\mathbf{x}^2) & ... & C_{m.f}(\mathbf{x}^N) \end{bmatrix}^T \tag{10}$$

which is a least-square optimal solution to the linear regression problems $[a_{d.0}\ a_{d.1}\ ...\ a_{d.n}\ d_{d.0}\ d_{d.1}\ ...\ d_{d.n}]^T\mathbf{C}_d = \mathbf{F}_d$ and $[a_{m.0}\ a_{m.1}\ ...\ a_{m.n}\ d_{m.0}\ d_{m.1}\ ...\ d_{m.n}]^T\mathbf{C}_m = \mathbf{F}_m$, equivalent to (5). Note that the matrices $\mathbf{C}_l^T\mathbf{C}_l$ and $\mathbf{C}_d^T\mathbf{C}_d$ are non-singular for $N > n +1$, which is the case for our choice of the training set.

Step 2: Construction of the response surface approximation (RSA) surrogate. Having the low-fidelity space-mapping-corrected, we sample the initial surrogate and create the RSA model of it. In this work, we use kriging

5

interpolation[10,11]. Given the training set $\mathbf{X}_{B.KR} = \{\mathbf{x}_{KR}^1, \mathbf{x}_{KR}^2, \ldots, \mathbf{x}_{KR}^{NKR}\} \subset \mathbf{X}_R$ be the base (training) set and $\mathbf{c}(\mathbf{X}_{B.KR})$ the corresponding low-fidelity model responses. The Kriging interpolant is derived as

$$\mathbf{s}_{KR}(\mathbf{x}) = \mathbf{M}\boldsymbol{\alpha} + \mathbf{r}(\mathbf{x}) \cdot \boldsymbol{\Psi}^{-1} \cdot (\mathbf{s}_0(\mathbf{X}_{B.KR}) - \mathbf{F}\boldsymbol{\alpha}), \tag{11}$$

where $\mathbf{M}$ and $\mathbf{F}$ are Vandermonde matrices of the test point $\mathbf{x}$ and the base set $\mathbf{X}_{B.KR}$, respectively. The coefficient vector $\boldsymbol{\alpha}$ is determined by Generalized Least Squares (GLS). $\mathbf{r}(\mathbf{x})$ is an $1 \times N_{KR}$ vector of correlations between the point $\mathbf{x}$ and the base set $\mathbf{X}_{B.KR}$, where the entries are $r_i(\mathbf{x}) = \boldsymbol{\Psi}(\mathbf{x}, \mathbf{x}_{KR}^i)$, and $\boldsymbol{\Psi}$ is a $N_{KR} \times N_{KR}$ correlation matrix, with the entries given by $\boldsymbol{\Psi}_{i,j} = \boldsymbol{\Psi}(\mathbf{x}_{KR}^i, \mathbf{x}_{KR}^j)$. In this work, the exponential correlation function is used, i.e., $\boldsymbol{\Psi}(\mathbf{x}, \mathbf{x}') = \exp(\sum_{k=1,\ldots,n} -\theta_k |x_k - x'_k|)$, where the parameters $\theta_1, \ldots, \theta_n$ are identified by Maximum Likelihood Estimation (MLE). The regression function is chosen constant, $\mathbf{F} = [1 \ldots 1]^T$ and $\mathbf{M} = (1)$.

Given the number design variables, 8 in this case, the design of experiments used at this step is LHS with 1,000 samples supplemented by design space corners (256 samples). Thus, the total number of training samples at this stage is 1,256.

Step 1 of the surrogate modeling process allows us to reduce misalignment between the low- and high-fidelity models. The surrogate model created in Step 2 is a response surface approximation one so that it is fast and yet accurate because relatively dense sampling of the design space is utilized. Nevertheless, the computational cost of constructing the surrogate is low because it is based on low-fidelity model data: the cost of 1,256 low-fidelity data samples is equivalent to just a few dozen of high-fidelity ones.

B. Surrogate Model Enhancement Using Co-Kriging

In this work, we use co-kriging[28] to iteratively enhance the surrogate model and refine the initial Pareto front representation found by the kriging surrogate constructed in the previous section. Generation of a co-kriging model is carried out through sequential construction of the two kriging models: the first model $\mathbf{s}_{KRc}$ composed from the low-fidelity training samples $(\mathbf{X}_{B.KRc}, \mathbf{s}_0(\mathbf{X}_{B.KRc}))$, and the second $\mathbf{s}_{KRd}$ model generated on the residuals of the high- and low-fidelity samples $(\mathbf{X}_{B.KRf}, \mathbf{s}_d)$, where $\mathbf{s}_d = \mathbf{f}(\mathbf{X}_{B.KRf}) - \rho \cdot \mathbf{s}_0(\mathbf{X}_{B.KRf})$. The parameter ρ is a part of MLE of the second model. In the absence of $\mathbf{s}_0(\mathbf{X}_{B.KRf})$, they can be approximated by the first model, i.e., as $\mathbf{s}_0(\mathbf{X}_{B.KRf}) \approx \mathbf{s}_{KRc}(\mathbf{X}_{B.KRf})$. Configuration (the choice of the correlation function, regression function, etc.) of both models can be adjusted separately for the corrected low-fidelity data $\mathbf{s}_0$ and the residuals $\mathbf{s}_d$, respectively. Moreover, both models use the exponential correlation function together with constant regression function $\mathbf{F} = [1 \ 1 \ldots 1]^T$ and $\mathbf{M} = (1)$.

The final co-kriging model $\mathbf{s}_{CO}(\mathbf{x})$ is defined similarly as in (11), i.e.,

$$\mathbf{s}_{CO}(\mathbf{x}) = \mathbf{M}\boldsymbol{\alpha} + \mathbf{r}(\mathbf{x}) \cdot \boldsymbol{\Psi}^{-1} \cdot (\mathbf{s}_d - \mathbf{F}\boldsymbol{\alpha}), \tag{12}$$

where the block matrices $\mathbf{M}$, $\mathbf{F}$, $\mathbf{r}(\mathbf{x})$ and $\boldsymbol{\Psi}$ of (12) can be written as a function of the two underlying Kriging models $\mathbf{s}_{KRc}$ and $\mathbf{s}_{KRd}$:

$$\mathbf{r}(\mathbf{x}) = [\rho \cdot \boldsymbol{\sigma}_c^2 \cdot \mathbf{r}_c(\mathbf{x}), \rho^2 \cdot \boldsymbol{\sigma}_c^2 \cdot \mathbf{r}_c(\mathbf{x}, \mathbf{X}_{B.KR_f}) + \boldsymbol{\sigma}_d^2 \cdot \mathbf{r}_d(\mathbf{x})]$$

$$\boldsymbol{\Psi} = \begin{bmatrix} \boldsymbol{\sigma}_c^2 \boldsymbol{\Psi}_c & \rho \cdot \boldsymbol{\sigma}_c^2 \cdot \boldsymbol{\Psi}_c(\mathbf{X}_{B.KR_c}, \mathbf{X}_{B.KR_f}) \\ 0 & \rho^2 \cdot \boldsymbol{\sigma}_c^2 \cdot \boldsymbol{\Psi}_c(\mathbf{X}_{B.KR_f}, \mathbf{X}_{B.KR_f}) + \boldsymbol{\sigma}_d^2 \cdot \boldsymbol{\Psi}_d \end{bmatrix} \tag{13}$$

$$F = \begin{bmatrix} F_c & 0 \\ \rho \cdot F_d & F_d \end{bmatrix}, \qquad M = [\rho \cdot M_c \ M_d]$$

where $(\mathbf{F}_c, \boldsymbol{\sigma}_c, \boldsymbol{\Psi}_c, \mathbf{M}_c)$ and $(\mathbf{F}_d, \boldsymbol{\sigma}_d, \boldsymbol{\Psi}_d, \mathbf{M}_d)$ of (13) are matrices obtained from the $\mathbf{s}_{KRc}$ and $\mathbf{s}_{KRd}$, respectively. Generally, $\boldsymbol{\sigma}_c^2$ and $\boldsymbol{\sigma}_d^2$ are process variances, while $\boldsymbol{\Psi}_c(\cdot,\cdot)$ and $\boldsymbol{\Psi}_d(\cdot,\cdot)$ stand for correlation matrices of two datasets with the optimized θ_k parameters and correlation function of $\mathbf{s}_{KRc}$ and $\mathbf{s}_{KRd}$, respectively.

C. Multi-objective Optimization Algorithm

The initial set of Pareto-optimal designs (Pareto set) is obtained by optimizing the surrogate model created as described in Sec. III.A. The surrogate is optimized in the multi-objective sense using a multi-objective evolutionary

algorithm (MOEA). Here, we use a standard multi-objective evolutionary algorithm with fitness sharing, Pareto-dominance tournament selection and mating restrictions[16]. The main changes (compared to single-objective evolutionary algorithms) are the mechanisms that push the solutions towards the Pareto front (here, realized through Pareto-dominance-based fitness function as well as the aforementioned selection procedure) and spread the solutions along the front (here, realized using fitness sharing and mating restrictions). The algorithm is modified in order to handle nonlinear constraints. The modification include: (*i*) initialization procedure that only generated feasible individuals, and (*ii*) crossover and mutation procedures that maintain feasibility of individuals. The details are omitted for the sake of brevity.

The entire design optimization flow can be summarized as follows:

1. Correct the low-fidelity model **c** using parameterized output space mapping as in (2);
2. Sample the design space and acquire the $\mathbf{s}_0$ data;
3. Construct the kriging interpolation surrogate model $\mathbf{s}_{KR}$;
4. Obtain the Pareto front by optimizing $\mathbf{s}_{KR}$ using MOEA;
5. Evaluate high-fidelity model at selected geometries from the Pareto front.
6. Enhance the surrogate model to create the co-kriging model $\mathbf{s}_{CO}$;
7. Obtain the updated Pareto front by optimizing $\mathbf{s}_{CO}$ using MOEA;
8. If the termination condition is not satisfied, go to 5.
9. END

Steps 1-4 of the above procedure lead to generating the initial approximation of the Pareto front. In Steps 5-8, the Pareto front is refined by incorporating the verification high-fidelity CFD data samples into the surrogate model using co-kriging. The high-fidelity model is only evaluated at Step 1 (to realize space mapping correction of the low-fidelity model; this step is optional and the algorithm may work directly with the "raw" low-fidelity model data as well) and Step 5. The high-fidelity samples obtained at Step 5 are also used for verification purposes: if the alignment between these samples and the surrogate ones is sufficient, the algorithm is terminated. In this work, we utilize 15 high-fidelity model samples in each evaluation of Step 5 of the process.

IV. Numerical Case Study

A. Description

To demonstrate how the methodology described in Section III works, we consider multi-objective airfoil design in transonic flow at fixed lift. In particular, the free-stream Mach number is set to $M_\infty = 0.734$, and lift coefficient constraint is fixed at $C_l = 0.824$. Two conflicting objectives are considered: drag minimization and pitching moment maximization, i.e., we have $F_1(\mathbf{x}) = C_{d.f}$ and $F_2(\mathbf{x}) = -C_{m.f}$. We use the B-spline parameterization approach, described in Sec. II.B, with 8 design variables. The baseline airfoil shape is the RAE 2822. The shape is fitted to a B-spline curve by setting the *x*-locations of design variables as $\mathbf{X} = [\mathbf{X}_u; \mathbf{X}_l]^T = [0.0\ 0.15\ 0.45\ 0.8;\ 0.0\ 0.35\ 0.6\ 0.9]^T$. After the fit, the baseline design variable vector is $\mathbf{x} = [\mathbf{x}_u; \mathbf{x}_l]^T = [0.0175\ 0.04975\ 0.0688\ 0.0406;\ -0.0291\ -0.0679\ -0.03842\ 0.0054]^T$. The lower and upper bounds of $\mathbf{x}$ are set as $\mathbf{l} = [0.0105\ 0.0414\ 0.0537\ 0.0200;\ -0.0369\ -0.0808\ -0.0666\ -0.0265]^T$ and $\mathbf{u} = [0.0231\ 0.0629\ 0.0889\ 0.0816;\ -0.0231\ -0.0536\ -0.0210\ 0.0140]^T$, respectively, and a cross-sectional area constraint is imposed as $A \geq A_{\text{RAE2822}} = 0.0779$. An initial base set of 1,283 airfoils is generated within the upper and lower bounds as described in Sec. III.A. Figure 4 shows the baseline airfoil as well as a few samples from the base set.
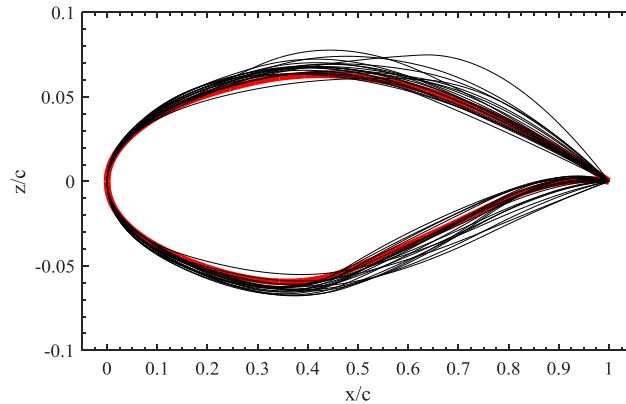

Figure 4.   The baseline airfoil RAE 2822 (red) and a few samples from the base set of airfoil shapes.

American Institute of Aeronautics and Astronautics

B. Results

The multi-objective optimization process has been executed as described in Section III.C. The results presented below have been obtained in four iterations of the algorithm. Figure 5 shows the Pareto fronts predicted by the surrogate model at iteration 1, 2 and 4, as well as the high-fidelity verification designs sampled along the front. It can be observed that the Pareto front (the best possible trade-off between the drag and pitching moment coefficients) predicted in the iteration if overoptimistic concerning the drag coefficient. Including high-fidelity model data through co-kriging modeling allows for improved prediction. After four iterations, the agreement between the predicted front and the verification samples is very good except its left-hand-side edge where the actual high-fidelity model samples exhibit higher drag. This would be corrected if a larger number of iterations have been executed. Figures 6 and 7 show the characteristics of a few airfoils along the final Pareto front in Fig. 5.

The overall computational cost of the multi-objective process is $27 + 1{,}256 = 1{,}283$ low-fidelity model evaluations (initial space mapping correction and kriging model construction) and $27 + 60$ high-fidelity model evaluations (space mapping correction and four iterations of co-kriging-based Pareto front refinement).
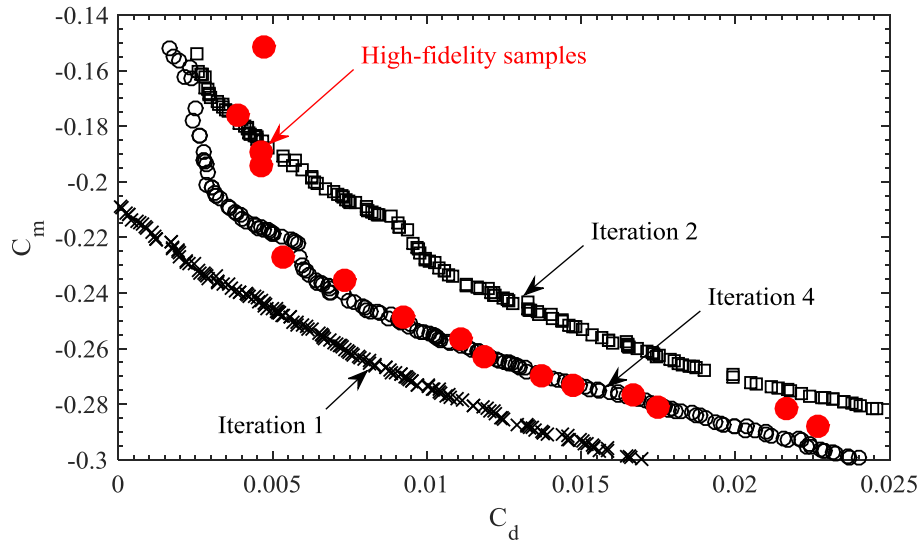

Figure 5. Pareto sets for a few iterations obtained by optimizing the surrogate (black symbols) at $M = 0.734$ and $C_l = 0.824$, and 15 high-fidelity evaluations sampled along the final Pareto front (red circles).
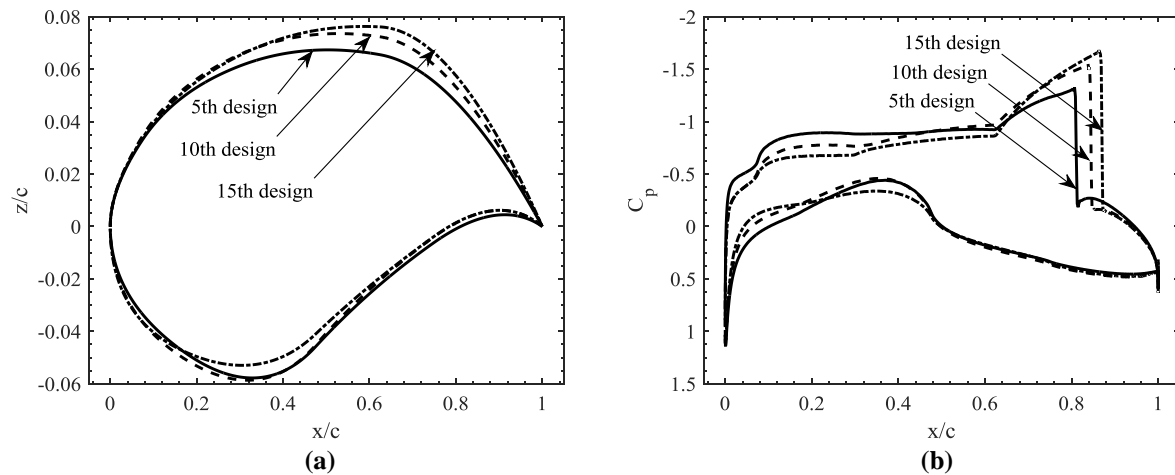

Figure 6. Characteristics of airfoils from design along the final Pareto front in Fig. 5 (enumerated starting from the left-most high-fidelity sample): (a) shapes, (b) pressure coefficient distributions.

American Institute of Aeronautics and Astronautics

(a) 5th design

(b) 10th design
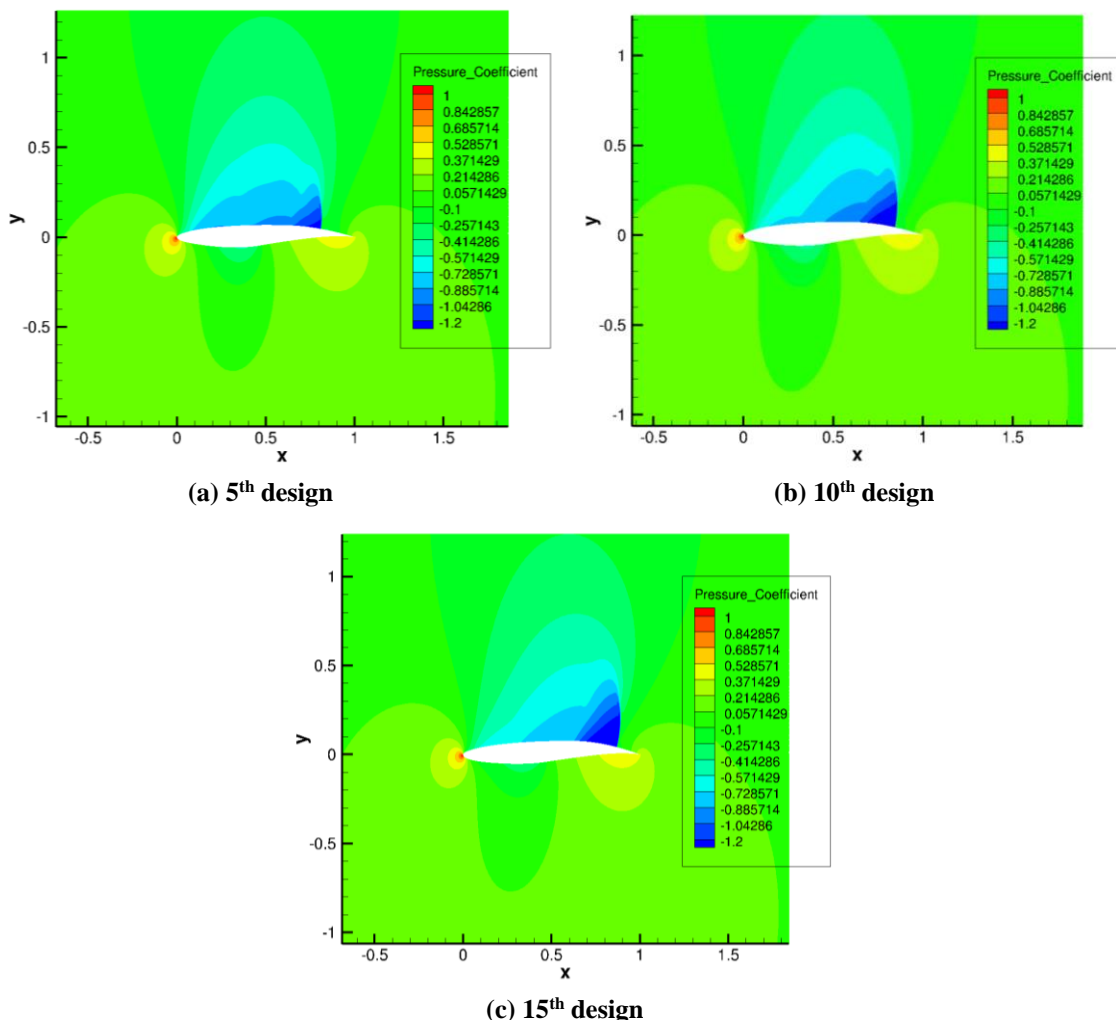

(c) 15th design

Figure 7. Pressure coefficient contours of the flow around the airfoils from design along the final Pareto front in Fig. 5 (enumerated starting from the left-most high-fidelity sample).

V. Conclusion

A computationally efficient procedure for multi-objective optimization of airfoils has been presented. The proposed approach exploits an auxiliary surrogate model created from kriging-interpolated low-fidelity CFD simulation data, as well as the multi-objective evolutionary algorithm that finds a set of designs representing the best trade-offs between design objectives. In order to improve the accuracy of the surrogate, the underlying low-fidelity model is corrected using parameterized output space mapping based on a limited number of high-fidelity CFD model evaluations. As a result of using the fast surrogate, the computational cost of finding the Pareto front is low.

References

[1]Leoviriyakit, K., Kim, S., and Jameson, A., "Viscous Aerodynamic Shape Optimization of Wings including Planform Variables," *21st Applied Aerodynamics Conference*, Orlando, Florida, June 23-26, 2003.

[2]Braembussche, R.A., "Numerical Optimization for Advanced Turbomachinery Design," In *Optimization and Computational Fluid Dynamics*, Thevenin, D. and Janiga, G., editors, Springer, 2008, pp. 147-189.

[3]Mader, C.A., and Martins, J. R. R. A., "Derivatives for Time-Spectral Computational Fluid Dynamics Using an Automatic Differentiation Adjoint," *AIAA Journal*, Vol. 50, No. 12, 2012, pp. 2809-2819. doi: 10.2514/1.J051658

[4]Mousavi, A., and Nadarajah, S., "Heat Transfer Optimization of Gas Turbine Blades Using an Adjoint Approach," *13th AIAA/ISSMO Multidisciplinary Analysis Optimization Conference*, AIAA Paper 2010-9048, Fort Worth, Texas, Sept. 13-15, 2010.

[5]Leung, T.M., and Zingg, D.W., "Aerodynamic Shape Optimization of Wings Using a Parallel Newton-Krylov Approach," *AIAA Journal*, Vol. 50, No. 3, 2012, pp. 540-550.

[6]Epstein, B., and Peigin, S., "Constrained Aerodynamic Optimization of Three-Dimensional Wings Driven by Navier-Stokes Computations", *AIAA Journal*, Vol. 43, No. 9, 2005, pp. 1946-1957.

[7]Nocedal, J., and Wright, S.J., *Numerical Optimization*, Springer, 2006.

[8]Kim, S., Hosseini, K., Leoviriyakit, K., and Jameson, A., "Enhancement of Class of Adjoint Design Methods via Optimization of Parameters", *AIAA Journal*, Vol. 48, No. 6, 2010, pp. 1072-1076.

[9]Schmidt, S., Gauger, N., Ilic, C., Schulz, V., "Three Dimensional Large Scale Aerodynamic Shape Optimization based on Shape Calculus", *41st AIAA Fluid Dynamics Conference and Exhibit*, AIAA Paper 2011-3718, Honolulu, Hawaii, June 27-30, 2011.

[10]Queipo, N.V., Haftka, R.T., Shyy, W., Goel, T., Vaidyanathan, R., and Tucker, P.K., "Surrogate-Based Analysis and Optimization," *Progress in Aerospace Sciences*, Vol. 41, No. 1, 2005, pp. 1-28

[11]Forrester, A.I.J., and Keane, A.J., "Recent advances in surrogate-based optimization," *Progress in Aerospace Sciences*, Vol. 45, No. 1-3, 2009, pp. 50-79.

[12]Koziel, S., Echeverría-Ciaurri, D., and Leifsson, L., "Surrogate-based methods," in S. Koziel and X.S. Yang (Eds.) *Computational Optimization, Methods and Algorithms*, Series: Studies in Computational Intelligence, Springer-Verlag, pp. 33-60, 2011.

[13]Alexandrov, N.M., Lewis, R.M., Gumbert, C.R., Green, L.L., and Newman, P.A., "Optimization with Variable-Fidelity Models Applied to Wing Design," *38th Aerospace Sciences Meeting & Exhibit*, Reno, NV, AIAA Paper 2000-0841, Jan. 2000.

[14]Robinson, T.D., Eldred, M.S., Willcox, K.E., and Haimes, R., "Surrogate-Based Optimization Using Multifidelity Models with Variable Parameterization and Corrected Space Mapping," *AIAA Journal*, vol. 46, no. 11, 2008.

[15]Booker, A.J., Dennis Jr., J.E., Frank, P.D., Serafini, D.B., Torczon, V., and Trosset, M.W., "A rigorous framework for optimization of expensive functions by surrogates," *Structural Optimization*, Vol. 17, No. 1, 1999, pp. 1-13.

[16]Fonseca, C.M., "Multiobjective genetic algorithms with applications to control engineering problems," PhD thesis, Department of Automatic Control and Systems Engineering, University of Sheffield, Sheffield, UK, 1995.

[17]Coello Coello, C.A., and Lamont, G.B., *Applications of Multi-Objective Evolutionary Algorithms*, World Scientific, 2004.

[18]Epstein, B., and Peigin, S., "Robust Hybrid Approach to Multiobjective Constrained Optimization in Aerodynamics", *AIAA Journal*, Vol. 42, No. 8, 2004, pp. 1572-1581.

[19]Nemec, M., Zingg, D.W., and Pulliam, T.H., "Multipoint and Multi-Objective Aerodynamic Shape Optimization", *AIAA Journal*, Vol. 42, No. 6, 2004, pp. 1057-1065.

[20]Koziel, S., Bekasiewicz, A., Couckuyt, I., Dhaene, T., "Efficient Multi-Objective Simulation-Driven Antenna Design Using Co-Kriging," *IEEE Tran. Antennas Propag.*, vol. 62, no. 11, pp. 5900-5905, 2014.

[21]Koziel, S., and Leifsson, L., "Knowledge-based airfoil shape optimization using space mapping," AIAA Paper 2012-3016, 30th *AIAA Applied Aerodynamics Conference*, New Orleans, Louisiana, June 25-28, 2012.

[22]Farin G., *Curves and Surfaces for Computer Aided Geometric Design*, Boston, MA: Academic Press, 1993.

[23]Palacios, F., Colonno, M. R., Aranake, A. C., Campos, A., Copeland, S. R., Economon, T. D., Lonkar, A. K., Lukaczyk, T. W., Taylor, T. W. R., and Alonso, J. J., "Stanford University Unstructured (SU^2): An open-source integrated computational environment for multi-physics simulation and design," AIAA Paper 2013-0287, 51st *AIAA Aerospace Sciences Meeting and Exhibit*, Grapevine, Texas, USA, 2013.

[24]Jameson, A., Schmidt, W., and Turkel, E., "Numerical Solution of the Euler Equations by Finite Volume Methods Using Runge-Kutta Time-Stepping Schemes," AIAA 1981-1259, *AIAA 14th Fluid and Plasma Dynamic Conference*, Palo Alto, CA, June 23-25, 1981.

[25]Pointwise V17.3R2, Pointwise Inc., 213 South Jennings Avenue, Fort Worth, Texas, 76104-1107, USA.

[26]Koziel, S., Cheng, Q.S., and Bandler, J.W., "Space mapping," *IEEE Microwave Magazine*, vol. 9, no. 6, pp. 105-122, 2008.

[27]Beachkofski, B., and Grandhi, R., "Improved distributed hypercube sampling," *American Institute of Aeronautics and Astronautics*, AIAA Paper 2002-1274, 2002.

[28]Forrester, A.I., Sobester, A., and Keane, A.J., "Multi-fidelity optimization via surrogate modelling", *Royal Society, Proceedings of the royal Society,* vol. 463, pp. 3251-3269, 2007.